

Cross-sectional transmission electron microscopy study of femtosecond laser- irradiated selenium-doped 'black' silicon

by

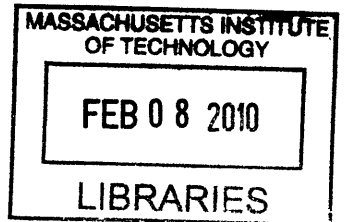
Arthur H. Reading

ARCHIVES

To the MIT Department of Materials Science and Engineering in partial fulfillment of the
requirements for the degree of Bachelor of Science in the field of Materials Science and
Engineering.

Massachusetts Institute of Technology
Cambridge, Massachusetts
May 2009

[June 2009]



The author hereby grants to MIT permission to reproduce and distribute publically paper
and electronic copies of this thesis document in whole or in part.

^ (1)

Signature of the author _____

Arthur H. Reading
Department of Materials Science and Engineering
May 8th, 2009

Certified by _____

Dr. Silvija Gradečak
Asst. Prof. of Materials Science and Engineering
Thesis supervisor

Accepted by _____

Dr. Lionel C. Kimerling
Prof. of Materials Science and Engineering
Chair, Undergraduate Committee

©2009
By Arthur H. Reading
All rights reserved.

Abstract

'Black silicon' refers to silicon that has been treated in a laser-ablation process to incorporate large amounts of chalcogen dopants. The material has been found to have greatly increased absorbance of visible and infrared wavelength light in comparison to undoped crystalline silicon.

Selenium-doped black silicon that had been annealed at different temperatures were studied using transmission electron microscopy (TEM) and electron diffraction. The goal of the investigation was to characterize the structure of the laser-altered regions of the material. In addition, energy-dispersive X-ray spectroscopy (EDX) was conducted in a scanning transmission electron microscope (STEM) in order to map spatial distribution of the selenium and the silicon were located within the material.

The results of the TEM study showed roughly conical peaks of varying shapes protruding about 1 μm from the surface of the material. The material is altered up to a depth of up to 1-2 μm , where polycrystalline or amorphous layers were observed. Electron diffraction studies revealed increased crystallinity in the annealed sample. A continuous, sharp interface between the affected region and unaltered substrate was found and particles of diameter 5-100 nm embedded within the silicon were observed.

The STEM-EDX studies showed that the selenium was dispersed inhomogeneously throughout the material. The selenium is concentrated near the interface of the unaltered Si substrate and the laser-altered layer and a high local concentration of selenium in the embedded particles was recorded.

The findings in this study provide a first look at the underlying structure of black silicon and will lead to future work characterizing the material.

Table of contents

<i>Abstract</i>	3
<i>Table of Contents</i>	4
<i>Acknowledgements</i>	5
1 Introduction	6
2 Background and experimental methods	8
2.1 Black silicon preparation	8
2.1.1 Introduction to black silicon.....	8
2.1.2 Black silicon preparation method.....	8
2.1.3 Annealing of black silicon samples.....	10
2.2 Sample preparation for transmission electron microscopy	11
2.2.1 Introduction.....	11
2.2.2 Preparation of wafer sandwich.....	11
2.2.3 Mechanical polishing.....	12
2.2.4 Ion-beam polishing.....	13
2.3 Transmission electron microscopy and related techniques	16
2.3.1 Basic principles.....	16
2.3.2 Mass-thickness contrast.....	19
2.3.3 Electron diffraction.....	19
2.3.4 Diffraction contrast.....	22
2.3.5 Scanning transmission electron microscopy.....	23
2.3.6 Energy dispersive X-ray spectroscopy.....	24
3 Results and discussion	27
3.1 Introduction	27
3.1.1 Sample selection.....	27
3.1.2 TEM investigation.....	28
3.2 TEM and electron diffraction results	29
3.2.1 As-prepared black silicon.....	29
3.2.2 Black silicon annealed at 700°C.....	32
3.2.3 Black silicon annealed at 950°C.....	35
3.2.4 Comparison of TEM and electron diffraction results.....	37
3.3 STEM and X-ray spectroscopy results	40
3.3.1 As-prepared black silicon.....	40
3.3.2 Black silicon annealed at 950°C.....	42
4 Summary and future work	46
4.1 Summary of findings	46
4.2 Future work	46
4.2.1 Cathodoluminescence microscopy.....	46
4.2.2 High-angle dark field STEM.....	47
4.2.3 Focused ion beam (FIB) sample preparation.....	47
References	49

Acknowledgements

I would like to acknowledge the work of Matt Smith, who contributed greatly in working together with me on this project, which was in many regards a joint effort. I would also like to thank my advisor Prof. Gradečak for starting me on this project and for providing me with her guidance and her huge wealth of knowledge that made this work possible. The help of Yong Zhang was essential to all the electron microscopy done in this study. I would like to thank him for the many hours of training and repairs on all the instruments that were necessary for this project. I would also like to thank Sung-Keun Lim for his advice on sample preparation techniques and electron microscopy. I would also like to acknowledge the great work of the Mazur group at Harvard for preparing the material and for providing me with a huge amount of background material and knowledge. Finally I would like to thank the members of the Buonassisi group at MIT for their insights and ideas for the research.

1 Introduction and motivation

Silicon is the most widely used semiconducting material in the world today. This is due to its natural abundance, ease of processing, favorable electronic properties and exhaustive characterization. Despite its many advantages, there are some concerns with the viability of silicon as a material for photovoltaic cells or photodetectors. Silicon is an indirect band-gap material, meaning that there is weak coupling between electron band-gap transitions and photon emission or absorption. Photodetectors are an essential part of photonic telecommunications systems, but conventional silicon photodetectors cannot detect light at the red and infrared wavelengths that are used in telecommunications because photons at these wavelengths have energy smaller than silicon's bandgap energy.

Furthermore, silicon's inability to absorb light in the infrared makes it very inefficient at collecting energy from sunlight. Silicon is still the most widespread material used in photovoltaic cells, but this is mostly because it is well characterized, nontoxic and naturally abundant; not because of its optical properties. Improving silicon's ability to absorb light at longer wavelengths would be a big step in improving the efficiency of silicon based photovoltaic cells.

So-called 'black' silicon is an altered form of silicon that displays outstanding optical properties. The material is created by irradiating a silicon substrate with repeated, yet extremely short pulses of laser light in the presence of a high concentration of a chalcogen (S, Se, Te). The high-energy laser ablates the silicon during the doping process. As the silicon cools it solidifies into an array of conical

peaks while absorbing high concentration of dopant. The black silicon has interesting electronic properties that can be altered by thermal annealing, as is discussed in Chapter 2.

In this thesis, black silicon is investigated using cross-sectional transmission electron microscopy and associated techniques (See section 2.3). The aim is to understand the microstructural evolution that is taking place in the formation of the black silicon peaks, which is a key step in explaining outstanding optoelectronic properties of this unique material. Also, we hope to understand the effect of the annealing temperature on the performance of the black silicon as a photoabsorber. We used chemical mapping techniques to find distribution of the chalcogen atoms; in this case selenium.

Selenium based black silicon was prepared and annealed by the Mazur group at Harvard University. The preparation of cross-sectional electron microscope samples was done at MIT using the facilities of the Center for Materials Science and Engineering (CMSE) and the Gradečak Group.

2 Background and Experimental Methods

2.1 Black silicon preparation

2.1.1 Introduction to black silicon

So-called 'black' silicon refers to silicon that has been altered through a femtosecond laser chalcogen doping process to absorb large quantities of visible and infrared light. The name results from the fact that the treated surface appears very dark gray on visual inspection, due to its ability to absorb visible wavelength light, as is shown in Figure 2.1.

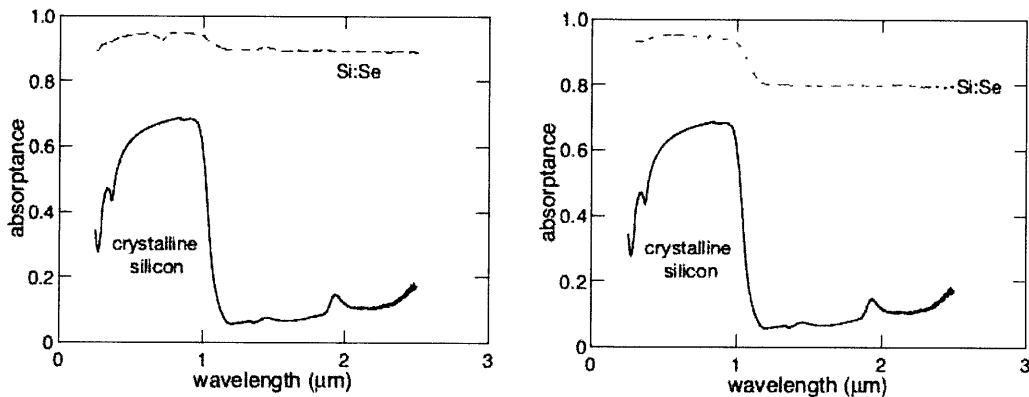


Fig. 2.1: Absorbance spectra of silicon irradiated with 100fs laser pulses focused to 10kJ/m^2 in the presence of selenium powder. Left: before annealing. Right: after annealing at 775K for 30 minutes. Si substrate is (111), *n*-type ($\rho = 800\text{-}1200\ \Omega\text{-cm}$). Data obtained from reference [1]

2.1.2 Black silicon preparation

The basic principle behind the preparation of black silicon is the use of a femtosecond laser to create an ultra-high-temperature mixture of silicon and a chalcogen at the surface of the sample. As the mixture cools, the material solidifies

into a state with a high concentration of chalcogen dopant [2]. In this investigation, selenium was used exclusively as the chalcogen dopant.

The substrates used for all samples were high-resistivity Si (100) wafers ($\rho = 3000\text{-}6000\Omega\text{-cm}$, n type doped with phosphorus). A 75nm layer of selenium was deposited directly onto the surface of the silicon wafers in a vacuum environment. The sample was kept in an inert N_2 at a pressure of 6.7×10^4 Pa. This created favorable hydrodynamics during the laser irradiation process. A diagram of the femtosecond laser irradiation apparatus is shown in Figure 2.2.

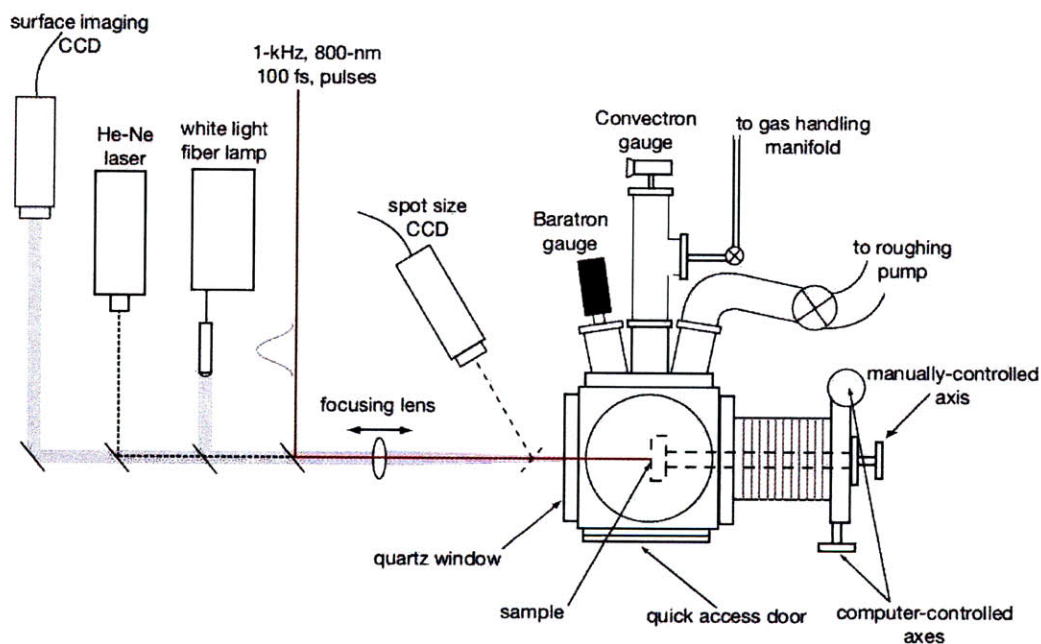


Fig. 2.2: Diagram of the femtosecond laser treatment apparatus. The same apparatus was used for all samples. The spot size was observed using a CCD camera. The laser irradiation procedure was conducted entirely in an inert environment. Diagram from reference [1].

The wafers were irradiated by laser light in 50-femtosecond long pulses of 800 nm light at a frequency of 25Hz. The fluence of the beam was 2kJ/m² and the beam was focused to a spot diameter of about 875μm. The surface of the sample was oriented perpendicularly to the incident laser beam. The beam was scanned across a 33×33mm area at a speed of 1.5mm/s. Under these conditions, every point on the surface of the sample received 175 laser pulses within the laser's full-width at half maximum intensity spot.

2.1.3 Annealing of black silicon

Thermal annealing has been found to profoundly affect the optical properties of black silicon, as is seen in Fig. 2.1. The annealing temperatures that were used for samples in this thesis were 700°C and 950°C. The annealing was done in an open-tube furnace in an inert atmosphere of 95% N₂, 5% H₂ gas. The annealed samples were placed into a preheated furnace at the desired temperature. After 30 minutes they were removed and allowed to cool in air at room temperature.

2.2 Sample preparation for transmission electron microscopy

2.2.1 Introduction

The goal of the sample preparation process is to create an electron-transparent sample that is mechanically stable to sustain manipulation and handling. A standard TEM sample is thinned by mechanical or chemical means and mounted on a copper grid or ring of 3mm diameter. In order to investigate the internal structure of the black silicon material across different thicknesses, it was necessary to create cross-sectional samples. This was accomplished in three steps: (1) creating a stable Si wafer ‘sandwich’ structure, (2) mechanical polishing using diamond lapping films, and (3) brief polishing using an ion mill. These steps are described in detail in sections 2.2.1-2.2.3 and in Figure 2.3.

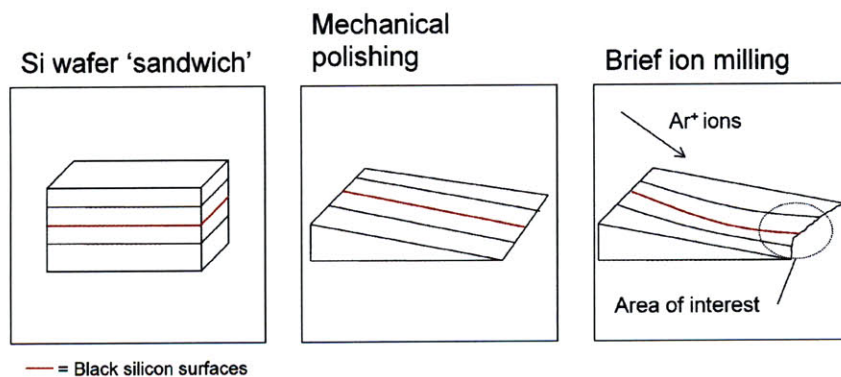


Fig. 2.3: Schematic of sample during TEM sample preparation process. The red line indicates the surface of black silicon. After ion milling, the sample was glued to a TEM grid (see Fig. 2.6)

2.2.2 Preparation of a wafer sandwich

In order to provide structural stability during the mechanical and ion polishing, a sandwich-like structure was made from two black silicon and two dummy silicon pieces of the same size (1mm x 3mm). The substrate cleaving was

accomplished using a diamond scribe and glass slides to ensure straight cuts. The two black silicon pieces were glued together with the surfaces of interest facing one another (see Fig. 2.3). Then the dummy silicon pieces were glued on either side to create the sandwich. In this way, the black silicon surface of interest was protected and maximized without sacrificing the overall structural stability. The glue that was used was Ted Pella M-Bond™ 610 Adhesive. This glue was chosen for its electron transparency and low viscosity, allowing very thin regions of glue in the resulting cross-sectional sample. After the gluing, the sample was compressed using spring-loaded tweezers in order to make the glue regions as thin and secure as possible, and dried overnight to ensure complete curing of the epoxy.

2.2.3 Mechanical polishing

The samples were polished mechanically using diamond lapping films and a Tripod polisher. A Tripod polisher is a stand with three Delrin feet that are attached to micrometers. The sample to be polished is mounted on a flat Pyrex stage using mounting wax. The mounting process involved melting the mounting wax at 400°C for approximately 5 minutes. Oxidation and annealing of the silicon during this process are assumed to be negligible due to the relatively low temperature and time. After the curing process had finished, the micrometers were adjusted so that the Pyrex holder and the rear Delrin feet are coplanar. The entire setup was rested on a moving polishing wheel to begin polishing. The advantage of a Tripod polisher

over a simple mounting block is that it allows very precise control of the wedge angle during polishing.

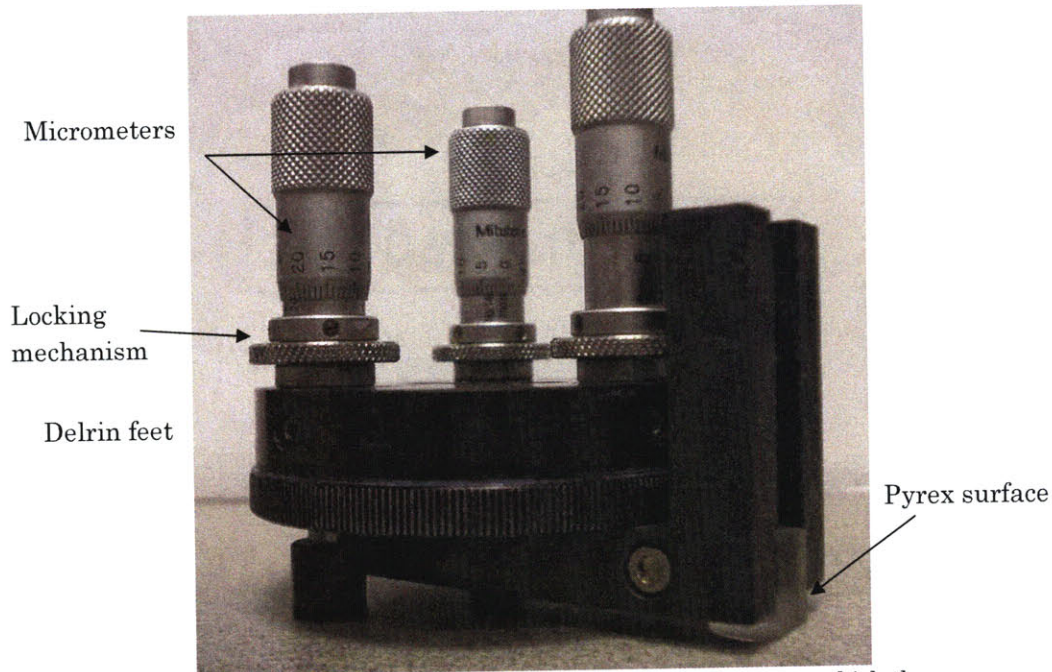


Fig. 2.4: Photograph of tripod polisher. The Pyrex surface onto which the sample is mounted is visible at the bottom right of the image. The three micrometers on the top extend the Delrin feet through the body of the device. The micrometers have a locking mechanism to fix their position.

Mechanical polishing consisted of two steps: first-side and second-side polishing. For the both steps, polishing films of decreasing grain size were used. The grain sizes used were 30, 15, 6, 3, 1 and $0.5\mu\text{m}$.

The aim of the first side polish was to obtain a flat surface by using each polishing film successively. The surface was then polished using a nylon-fiber polishing mat immersed in a suspension of $0.1\mu\text{m}$ diamond particles. After a flat, scratch-free surface had been achieved the sample was turned around with the smooth side facing into the sample holder, covered in mounting wax. Then the same

diamond lapping film sequences was used to thin the sample to near electron transparency, as follows. The rear micrometers of the Tripod polisher were extended 100 μ m. This caused the polishing to be at an angle. After second-side polishing, the sample was in the shape of a wedge (see Fig. 2.3) that was 10-15 μ m at its thickest point and 2-3 mm long. The approximate thickness of the silicon at this stage was determined by its color in transmission optical microscopy, with a dark red color indicating 10 μ m thickness and yellowish white with interference fringes indicating sub-micron thickness.

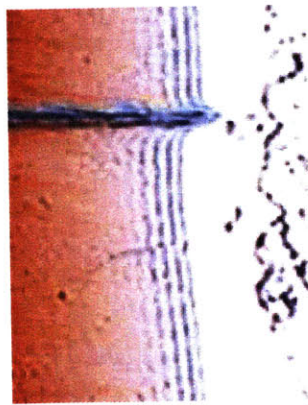


Fig. 2.5: Thickness fringes in a silicon wedge. The reddish coloration increases with thickness of the silicon until approximately 10 μ m, when it becomes opaque. Image taken from reference [8].

After polishing the sample was mounted onto a copper ring with a 90° arc cut out using a razor blade. This arc was cut out so as not to block the ion beam during ion beam polishing (see Fig. 2.6). The ring was mounted using a fast-curing 2-part epoxy.

2.2.4 Ion beam polishing

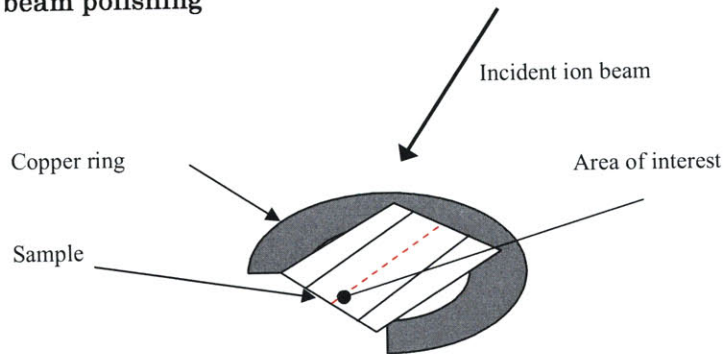


Fig. 2.6: Diagram of ion milling setup. Incident beam energy was 5keV at 5° from horizontal. The dashed line indicates the black silicon surfaces. The ion milling was conducted for approximately 15min in order to

After the mechanical polishing the samples were thinned in a Gatan Precision Ion Polishing System (PIPS). The ion beam consisted of argon ions accelerated at 5kV operating voltage. The goal of the ion milling was to further thin the thinnest part of the wedge-shaped specimen to electron transparency. Two ion beams, positioned at the same angle, were used in the ion milling process; one above and one below the sample. During milling, the sample was steadily rotated in order to reduce the likelihood of damage from the ion beam ‘burning’ into the sample. The two beams were synchronized to this rotation so that milling proceeded only while the sample was positioned with the thinnest region pointing away from the ion source. This preserved the stability of the wedge shaped sample. The samples were polished for approximately 15 minutes at an incident beam angle of 5° from horizontal, and were monitored in an optical microscope throughout. Contamination from the ion beam under these conditions was assumed to be minimal, due to the small amount of time spent under the ion beam [9].

2.3 Transmission Electron Microscopy and Related Techniques

2.3.1 Basic principles

Transmission electron microscopy (TEM) is a technique that provides structural and chemical information from a thin specimen by scattering a beam of high energy (100 – 300keV) electrons through it. The TEM can be used for both imaging and electron diffraction analysis. The major components of a TEM are an electron source, the electromagnetic lenses for focusing the electron beam, a movable sample stage, a vacuum system and the electron detector(s).

The electron gun provides a source of electrons. In a thermionic electron source, a tungsten or LaB₆ filament is electrically heated so that it emits electrons. In a field emission source, electrons are emitted by quantum tunneling from a very fine tipped tungsten cathode. The quantum tunneling is made possible by the high electric field at the tip of the source. The electrons are then accelerated downward by an anode plate kept at a high voltage relative to the filament. The result is a beam of accelerated electrons directed towards the sample and the electron detectors below.

The electron beam is focused by means of electromagnetic lenses consisting of copper coils within a solid pole-piece. Electrons, being negatively charged, are deflected by Lorentz forces in the presence of a magnetic field.

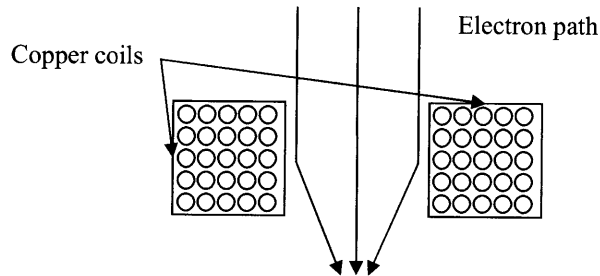


Fig. 2.7: Schematic of an electron lens. Electrons further from the center are deflected towards the center of the lens. This acts as a convex optical lens does for light, focusing the beam of electrons.

The magnetic field in the lens is rotationally symmetric around the axis of the microscope. The intensity of the magnetic field is such that electrons far from the axis are deflected more, creating an effect similar to light in a convex lens. By adjusting the current in the lens it is possible to change the focal length of the lens.

The main lenses in a TEM are the condenser lens, the objective lens, the intermediate lens and the projector lens. These, with the exception of the condenser lens, are shown in Fig. 2.8.

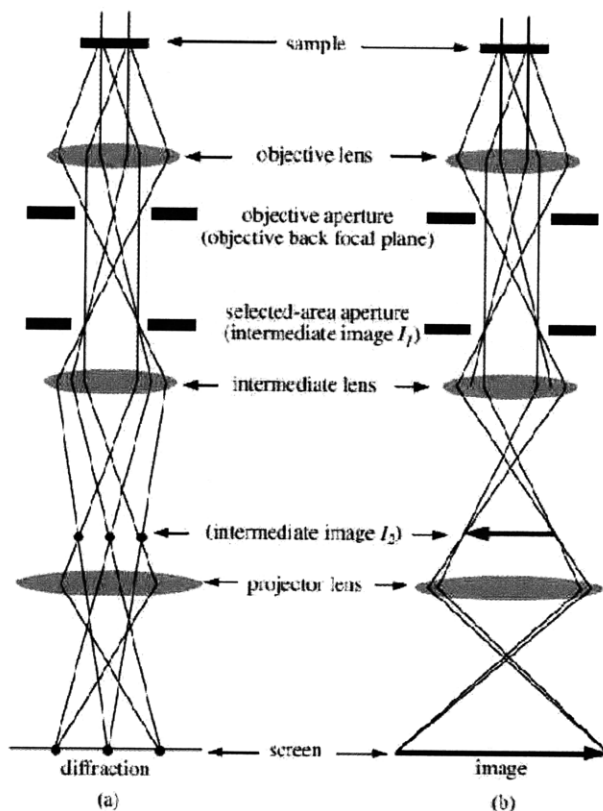


Fig. 2.8: Ray diagrams of TEM (a) electron diffraction mode and (b) imaging mode. The intermediate lens current is adjusted to switch between these imaging modes. Note also the positions of the apertures that are used for electron diffraction and bright-field imaging (see Sec. 2.3.3 and 2.3.4). Diagrams taken from [4]

The condenser lens is positioned above the sample in the microscope and serves to focus the beam along the optic axis of the microscope at the specimen. The result is a beam of electrons travelling parallel to the optic axis towards the sample. The electrons are diffracted by the sample and a diffraction pattern, consisting of multiple diffracted beams, is formed in the back focal plane of the objective lens, which is positioned below the sample. These beams combine to form a first image above the intermediate lens. The intermediate lens then focuses the beam such that

either the diffraction pattern or the image becomes the object of the projector lens. The projector lens then focuses the image or the diffraction onto the viewing screen at the bottom of the microscope.

The viewing screen is used to focus and view the image during microscopy. To record images the screen is lifted and the electron beam is allowed to expose either a photographic film or, more commonly, a CCD camera.

2.3.2 Mass-thickness contrast

There are several possible sources of contrast in TEM images. The most basic of these is known as mass-thickness contrast. Regions of a sample that have a higher average atomic number appear darker in a bright-field TEM image because they are more likely to scatter the incident electrons that are used to form the TEM image. Thicker regions of a sample similarly will scatter electrons. Mass-thickness contrast generally gives a qualitative view of a sample and allows basic observation of a sample's features. The other main type of contrast in TEM images of crystalline samples is diffraction contrast, which is described in section 2.3.4.

2.3.3 Electron diffraction

The wavelength, λ , of an electron is crucial in determining how an electron will be diffracted by a crystal. It is given by the De Broglie relation:

$$\lambda = \frac{h}{p}, \quad (2.1)$$

where h is the Planck constant and p is the relativistic momentum of an accelerated electron. An electron of rest mass m and charge e , accelerated by a voltage of E has a wavelength given by:

$$\lambda = \frac{h}{\left[2meE\left(1+\frac{Ee}{2mc^2}\right)\right]^{1/2}}, \quad (2.2)$$

where c is the speed of light. The accelerating voltage used in all experiments in this study was 200kV. Thus, the initial wavelength of all electrons used was 2.5pm.

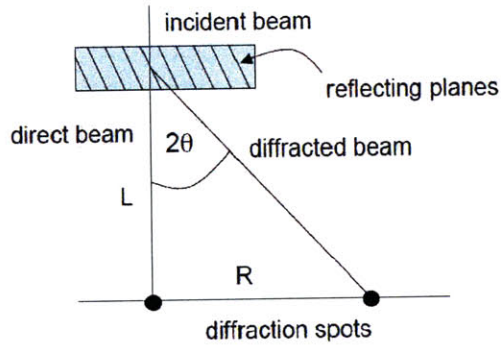


Fig. 2.9: Schematic of electron diffraction geometry. Here, θ is the diffracting angle, R is the diffraction spot spacing and L is the camera length of the microscope. Diagram from reference [10].

Diffraction refers to the interference between the plane wave of incident electrons and collective wavefunctions of electrons scattered from the atomic potentials in a sample. The angle at which the electrons diffract can be calculated for a given lattice spacing in a sample (see Fig. 2.9). For the electron wavefunctions to interfere constructively, the Bragg condition (Eq. 2.3) must be met.

$$2d \sin \theta = n\lambda \quad (2.3)$$

Here, θ is the angle of diffraction, d is the spacing between lattice planes, and n is an integer. The angle θ is very small in TEM electron diffraction, so the small angle approximation can be applied. The camera length L in a TEM is a representation of the effective distance from the sample to the viewing screen. It is not a physical distance, but must be quantified for a particular microscope by using known control samples. Therefore, $\sin(\theta) \approx L/R$, where R is the distance between the diffracted and transmitted beams when they reach the viewing screen. Eq. 2.3 then becomes Eq. 2.4.

$$\frac{R}{L} = \frac{\lambda}{d} \quad (2.4)$$

By analyzing the spacing of the diffracted spots, as shown in Fig. 2.4, we can obtain information about the crystal structure of a sample.

The main use of electron diffraction analysis in this thesis is to distinguish between crystalline and polycrystalline regions of the sample. A single-crystalline region of a sample will have a very regular pattern of spots, each of which can be attributed to a specific point in the reciprocal lattice of the crystal. In a polycrystalline sample, many crystals with different crystal orientations, but with the same unit cell dimensions. This has the result that polycrystalline diffraction patterns consist of a series of concentric rings, each of which with a radius that is inversely proportional to the different possible lattice spacings.

2.3.4 Diffraction contrast imaging

Diffraction contrast is achieved by specifically selecting the transmitted and/or diffracted beams that are formed in the back focal plane of the objective lens in order to form a bright-field or a dark-field image, respectively. This is accomplished by viewing the diffraction pattern of a sample and inserting an aperture into the back focal plane such that only one of the diffraction spots is visible. After the aperture has been positioned, the microscope is switched to imaging mode. Because only one beam is selected to form an image, there is increased contrast between regions that diffract in different ways. Take for example a sample where there are two adjacent regions of identical elemental composition with different electron diffracting conditions (e.g. different crystalline orientation). If an image is formed using the diffracted beam from only one of these regions, there will be contrast observed between the two regions. This is known as the diffraction contrast.

In so-called bright field microscopy, the transmitted beam is used to form an image. It is also possible to use an objective aperture to exclude the transmitted beam from contributing to the image and to only allow a diffracted beam to proceed through to the projector lens. This is known as dark field microscopy. Dark field microscopy is useful because it allows the identification of regions in an image that result from a specific diffracted beam in the diffraction pattern.

In this investigation, 'dirty' dark field microscopy is used. This name arises from the fact that the diffracted beam that was used for imaging was not traveling

down the optic axis of the microscope, as is the case in conventional dark-field imaging. The advantage of dirty dark field is that it does not require tilting of the electron gun such that the diffracted beam travels down the optic axis of the microscope. The drawback is that there is poorer resolution, due to the imperfections of electron lenses further away from the optic axis.

2.3.5 Scanning transmission electron microscopy (STEM)

Scanning transmission electron microscopy (STEM) is a technique where a beam of electrons is scanned across a specimen and the signal of transmitted electrons is measured below the sample. The advantage of STEM is that the resulting images are easier to interpret visually than regular TEM. This is because the images result from a beam of incoherent electrons, which reduces complicated effects like diffraction contrast. Additionally, it is relatively simple to ensure that the observed contrast in an image results from a variation of the average atomic number in different regions of the sample.

There are two main types of STEM that were used in this investigation: bright-field and dark-field STEM. A schematic of the detector geometry of these modes is shown in Fig. 2.10.

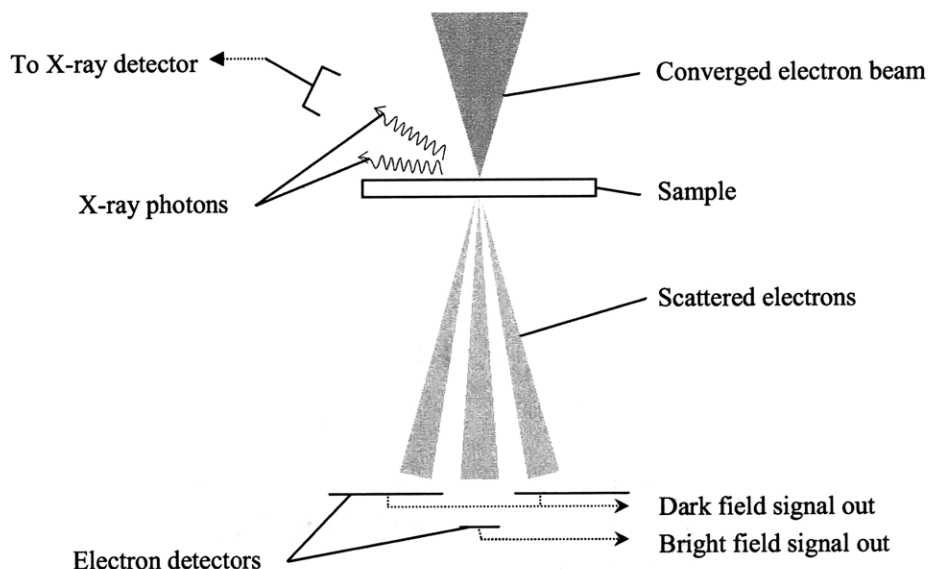


Fig. 2.10: Diagram of basic STEM imaging modes. Note that the dark field signal does not include the portion of the beam scattered at low angles.

As the beam is scanned across the sample, the electron detectors supply a current signal which is amplified and coupled to the scan rate of the electron beam to form an image; similar to conventional scanning electron microscopy.

A typical dark field detector is ring shaped and placed around the transmitted beam to gather scattered electrons in a rotationally homogenous fashion.

2.3.6 Energy dispersive X-ray spectroscopy

Energy-dispersive X-ray spectroscopy (EDX) is a technique that involves collecting and analyzing X-rays that are emitted from a sample in during STEM

operation. The X-rays that are emitted are the result of core-shell electron excitations in atoms in a sample. Every element has different characteristic X-ray energies that are observed in the spectrum of collected X-rays. This makes EDX a powerful technique for understanding the spatial distribution of different elements within a sample when the X-ray signal is coupled with the STEM image. This allows the creation of element ‘maps’ which can show where specific elements are located within an image.

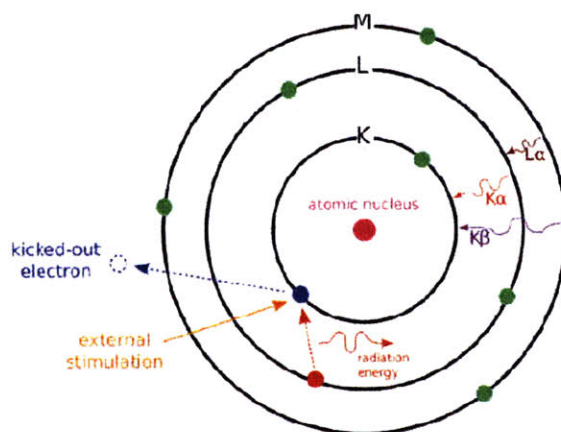


Fig. 2.11: X-ray excitations in an atom due to incident electrons. Note how all energy transitions are labeled using $K\alpha$, $K\beta$, $L\alpha$, etc. Diagram from reference [11]

In some cases, multiple elements will have characteristic X-ray energies that are very close together, making it difficult to distinguish between elements. Therefore it is essential to look for not only *one* characteristic X-ray emission, but for several energy peaks. For example, if a peak is observed at the characteristic $L\alpha$ energy of a given element, it is important to look for other characteristic peaks in the spectrum, such as $K\beta$ or $K\alpha$ in order to definitively identify that element.

To aid the analysis of X-ray spectra, the Oxford Instruments INCA computer program is used. This program features a database of all characteristic energy levels and a peak deconvolution algorithm that allows analysis of peaks that are overlapping. A peak is considered statistically significant if the following condition is met:

$$S_A > 3\sqrt{S_B}, \quad (3.5)$$

where S_A is the total number of X-ray counts inside the peak and S_B is the total number of background counts within the peak. This becomes important in assessing the significance of smaller peaks.

In STEM EDX, it is common to have rather low signals and acquisitions are made over periods of time. It is always possible that during this time a specimen has drifted, causing a blurring effect. The microscope used in this investigation did not appear to have noticeable sample drift during the times over which EDX maps were acquired (20min–1hr).

Chapter 3: Results and discussion

3.1 Introduction

3.1.1 Sample selection

A major part of the work in this study was to develop the sample preparation methods described in sections 2.2-2.3. Despite being repeated multiple times, the process was still prone to failure due to the extreme fragility of electron-transparent silicon samples. Once the sample preparation process had been established, three samples were successfully prepared (see 2.2) and investigated. Details of the samples are outline in Table 3.1.

Table 3.1: List of samples

Sample name	Annealing conditions
A	As-prepared
B	Annealed for 30min at 700°C
C	Annealed for 30min at 950°C

The samples were each prepared using the method described in Sections 2.2-2.3. Annealing of the black silicon has previously been found to have a profound impact on its optical and electronic properties [1], which is why the differently annealed samples were of interest. Preliminary measurements of the carrier concentration in the silicon were conducted by the Mazur group at Harvard University. These found that the black silicon had the highest carrier concentration after annealing at 700°C. Higher annealing temperatures were found to decrease the carrier concentration. This is why the 3 samples listed in Table 3.1 were selected for

structural investigation. The goal was that the TEM analysis would shed light on why the properties of black silicon changed with the annealing temperature.

3.1.2 TEM investigation

Each sample was first investigated with conventional bright-field TEM imaging (see 2.3.1) in order to characterize the crystallinity and general morphology. Selected-area electron diffraction (see 2.3.3) was used to assess the degree of crystallinity of the samples. The microscope used for the bright-field imaging and electron diffraction was a JEOL 2011 TEM with a LaB₆ thermionic electron gun, operating at 200kV accelerating voltage. Bright-field images were recorded using a CCD camera below the viewing screen. Electron diffraction patterns were taken using photographic film, which has a logarithmic dependence on image intensity. This allowed imaging of diffraction patterns with large differences in intensity. The bright field and electron diffraction results are shown in section 3.2.

The initial bright-field imaging revealed somewhat ambiguous results. In many cases, it was impossible to distinguish between diffraction contrast, thickness contrast, and chemical contrast. Therefore dark-field STEM (see 2.3.4) with EDX mapping (see 2.3.5) was used to obtain information about the chemical composition of the sample. The microscope used for the STEM analysis was a JEOL 2010F, using a field-emission electron gun with 200kV accelerating voltage. The STEM and EDX results are shown in section 3.3.

3.2 Bright field and electron diffraction TEM results

3.2.1 Sample A: As-prepared black silicon

First we will look at bright-field TEM images of sample A, the as-prepared material.

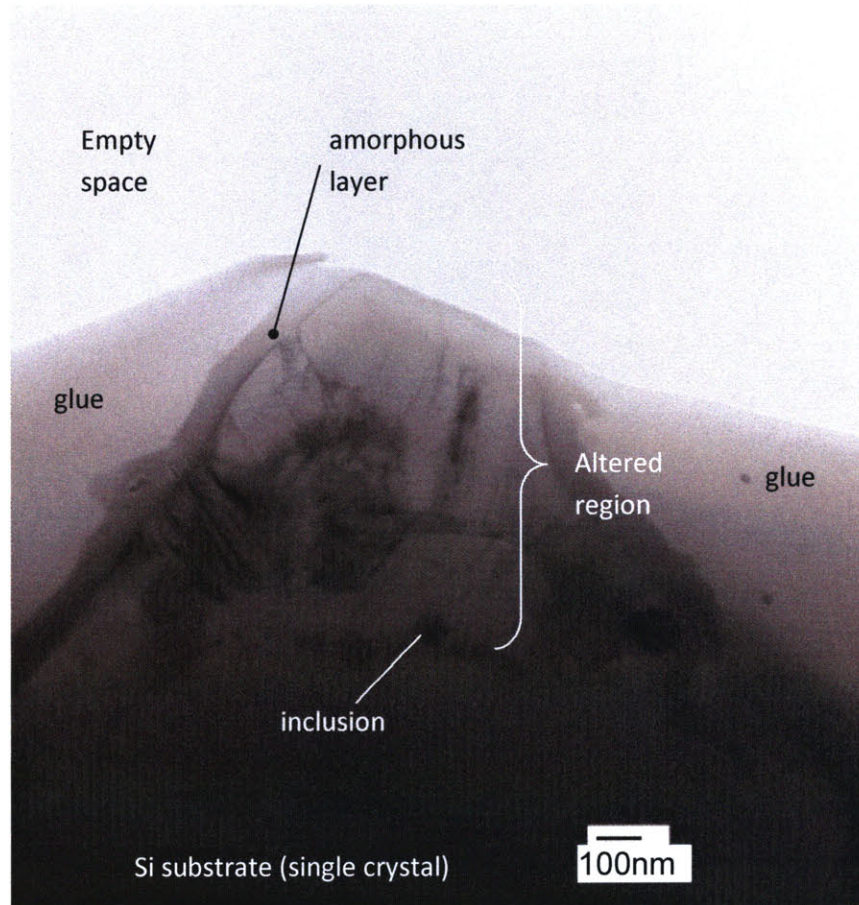


Fig. 3.1: Representative TEM image of as-prepared material. The overall structure is shared across many peaks in one sample, with the glue on either side of a peak. Notice how the glue has been removed due to the ion-beam thinning. The absence of the glue layer serves as a guide to where the tip of the black silicon peak has been milled away (see Section 2.2.4).

Fig. 3.1 shows a cross-section of an individual black silicon peak embedded in a layer of glue. The glue is visible as a relatively electron transparent region on either side of the triangular peak. There is a 50-100 nm thick layer of amorphous material on the surface of the material. The altered region of the black silicon

appears to penetrate a depth of about 500 nm into the surface of the sample, after which the silicon substrate appears largely unaltered. The tip of the peak seems to consist of a number of silicon grains with diameters ranging from around 100-300 nm. Interestingly, it appears that there are some dark inclusions of diameter less than 50 nm near the interface of the structured and unaltered regions. The darker contrast in these regions suggests a greater degree of electron scattering, possibly due to a higher average atomic number in these inclusions.

Due to diffraction contrast, grains of different crystal orientation will appear lighter or darker depending on their diffracting conditions. The diffracting conditions change when the sample is tilted inside the microscope. This makes it possible to distinguish areas with different crystal orientations, i.e. separate grains, as seen in Fig. 3.2.

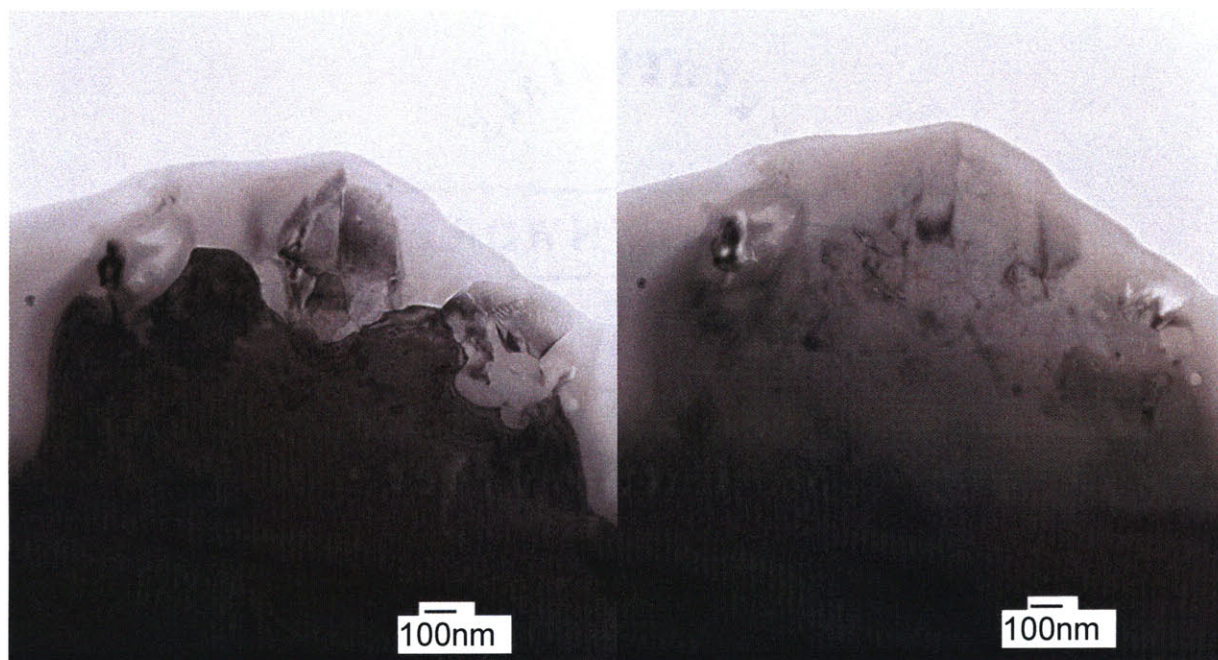


Fig. 3.2: As-prepared black silicon. The same peak imaged at different sample tilts. Note the strong difference in contrast between the images arising from diffraction contrast.

These images show exactly the same peak but at different tilts in the microscope. Tilting the sample changes the diffracting conditions of the differently oriented silicon grains in the peak. This allows us to distinguish between diffraction contrast and actual mass-thickness or chemical contrast.

Fig. 3.3 shows an electron diffraction pattern of a representative peak found in the as-prepared sample. Notice that the pattern is what one would expect from a polycrystalline material, i.e. one where the lattice parameters are the same throughout, but with regions of different crystal orientation within the selected area.

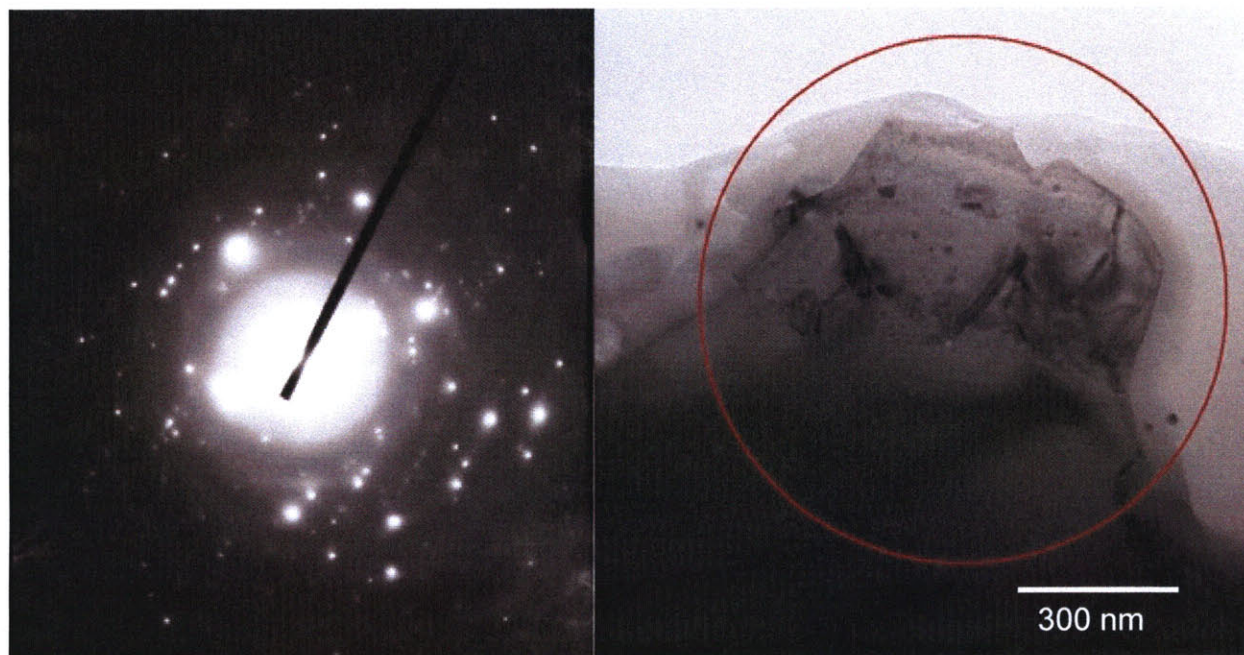


Fig. 3.3: Selected-area diffraction pattern (left) of a peak region (right) in as-prepared material. The pattern exhibits rings that are characteristic of a polycrystalline material. The dark line extending into the pattern on the left is a physical strip inserted to prevent overexposure of the film by the transmitted beam.

The irregularity of the diffraction pattern to the left in Fig. 3.3 suggests that the selected area contains multiple crystal orientations. This indicates that the material is polycrystalline [5].

3.2.2 Sample B: Black silicon annealed at 700°C

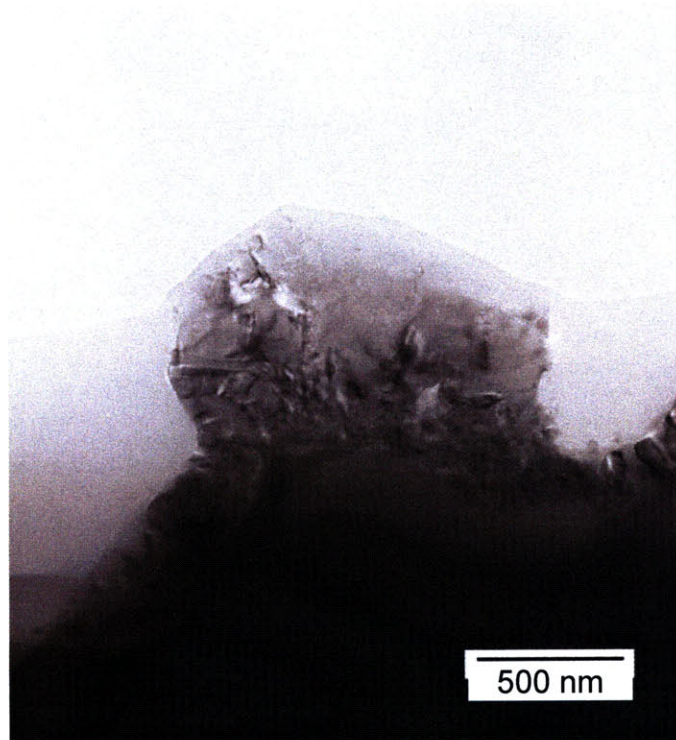


Fig. 3.3: Typical peak found in the black silicon annealed at 700°C. The sample annealed at 700°C seemed to have large altered regions.

The sample that was annealed at 700°C generally exhibited a microstructure similar to the as-prepared material. There appeared to be a continuous layer of altered material that continued between peaks, as can be seen on either side of the peak in Fig. 3.3. As with the as-prepared material, there was a clear interface between the single-crystalline silicon substrate and the altered region that was affected by the ablation treatment.

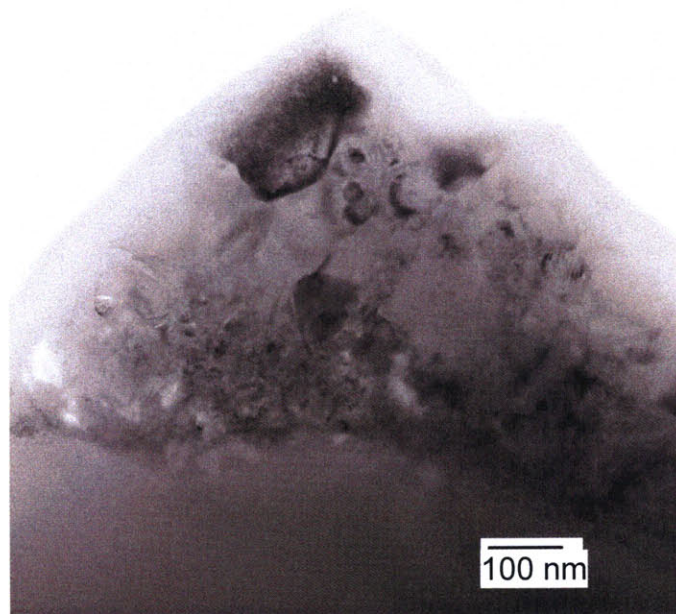


Fig. 3.4: Another peak region found in the 700°C annealed material. Note the difference in shape between this peak and the other one in the same sample. The peak region appears to contain a number of grains, which can be seen in Fig. 3.5

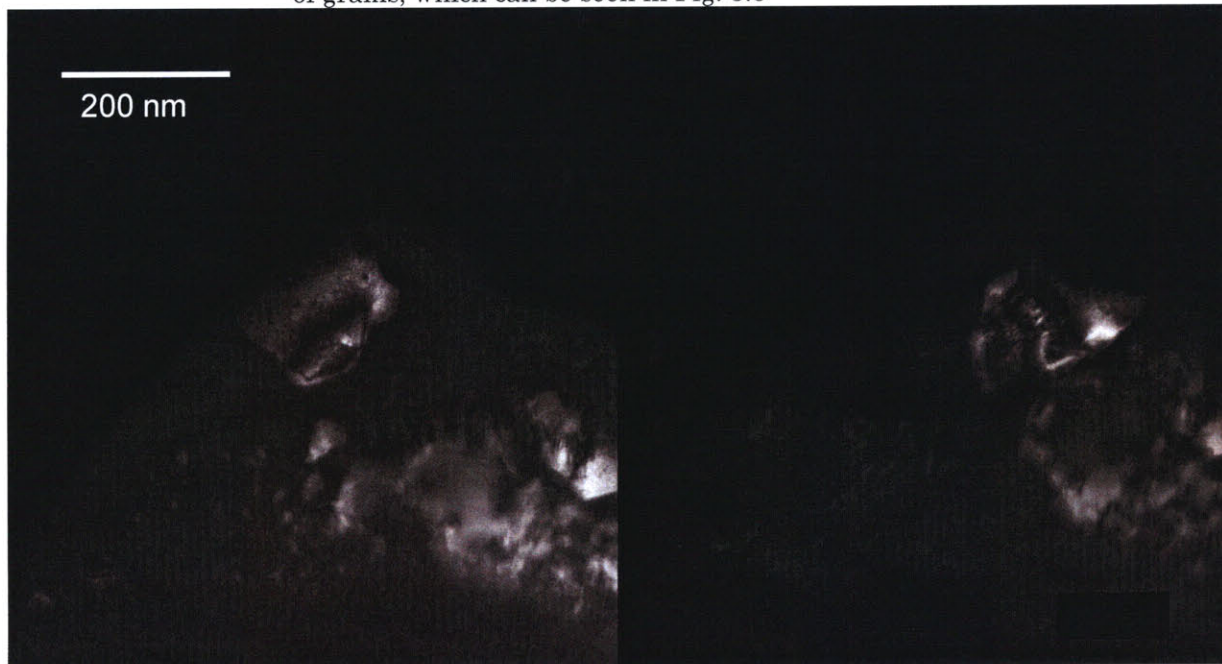


Fig. 3.5: 'Dirty' dark-field images of the same peak as found in Fig. 3.4 but using different diffracted beams. Grains with different crystal orientation tend to glow depending on whether their diffracted beam was used to make the image. Notice the poor resolution resulting from lens aberration away from the optic axis of the microscope.

The polycrystalline structure of the peaks was further confirmed using ‘dirty’ dark field microscopy (see section 2.3.3). Fig. 3.4 shows a bright field image of a typical peak in the sample. Fig. 3.5 shows the same peak but in dark field mode such that different grains in the polycrystalline region appear to glow. The grains do not share the same crystal orientation. Thus they diffract the electron beam in different directions. When the objective aperture is moved to select different diffracted beams instead of the transmitted beams, different grains will appear to glow based on whether one of their diffracted beams had been selected by the objective aperture to form the dark-field image. In this way we can distinguish between individual grains, similar to in Fig. 3.2 where sample tilt achieved a similar effect.

It should also be noted here that the peaks observed have rather different shapes. The peak in Fig. 3.4 has a decidedly pointed structure, whereas the peak in Fig. 3.3 appears to be more bulbous and rounded. The variation in peak shape within one sample was considerable, showing that the black silicon treatment is not homogenous across an entire sample, which complicates modeling of the solidification processes involved in creating the black silicon.

3.2.3 Sample C: Black silicon annealed at 950°C

The sample of black silicon annealed at 950°C appeared somewhat different than the sample annealed at 700 °C and the as-prepared sample. There seemed to be discontinuity of the structured layer between separate peaks.

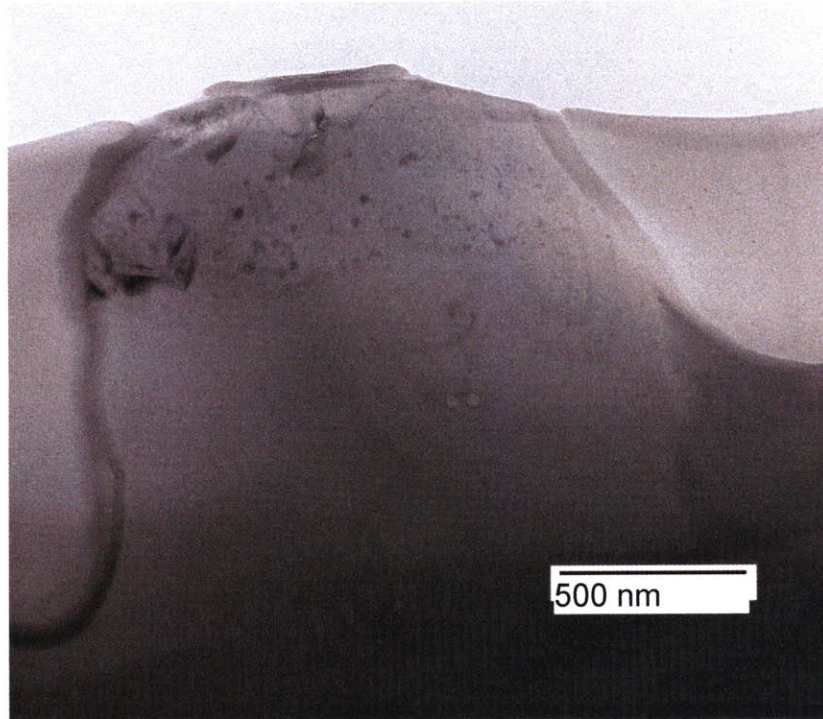


Fig. 3.6: A typical peak found in the black silicon annealed at 950°C. Note the relatively large single-crystalline region. The altered black silicon region does not appear to extend beyond the peak tip. Image courtesy Matt Smith.

In Fig. 3.6 we see a fairly large region of single-crystalline silicon below the layer of structured material. Also, it appears that there are fewer visible grains on order of 100-300 nm that are found in the other samples. This allows clearer imaging of the dark inclusions or precipitates that are found in the peaks.

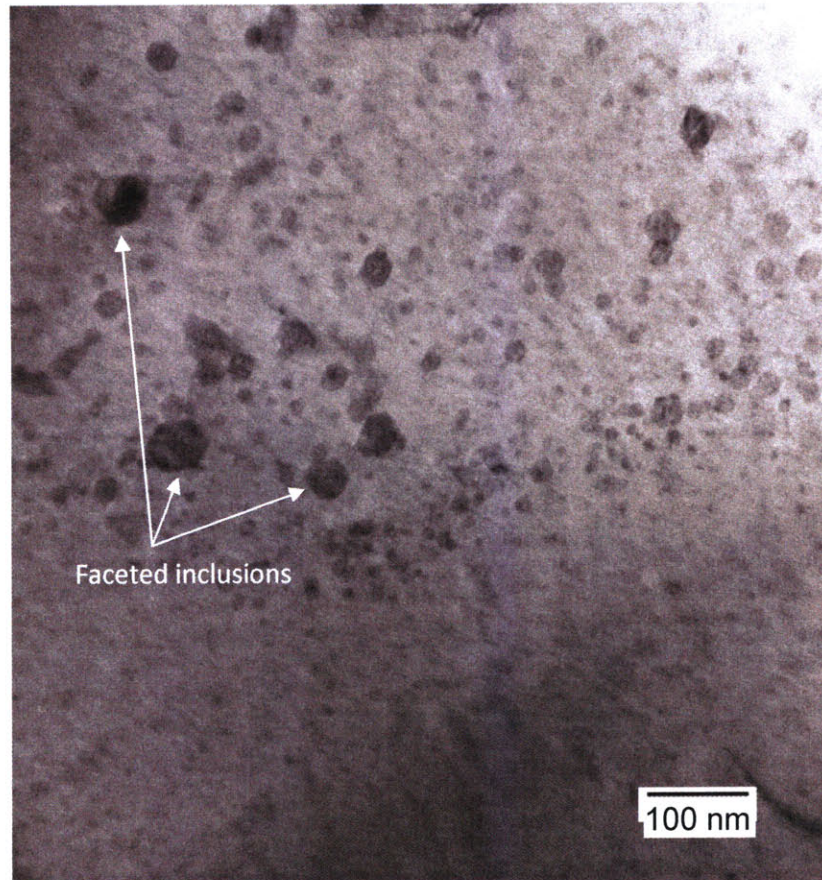


Fig. 3.7: Close-up bright field image of the inclusions found in Fig. 3.6. One can see a tendency to form facets, which indicates possible phase segregation taking place. The particles have diameters in the range 5-200 nm. Image courtesy Matt Smith.

The dark inclusions, or precipitates, seen in Fig. 3.7 show a faceted shape. These regions also remained dark when the sample was tilted, excluding the possibility of their dark contrast resulting from diffraction contrast. Therefore it is likely that their dark color arises from chemical contrast. Selenium has a higher atomic number than silicon, so regions with high concentrations of selenium would appear darker than regions of pure silicon when only chemical contrast is considered. These inclusions will be investigated further in the X-ray mapping in section 3.2 in order to discover more about their chemical composition.

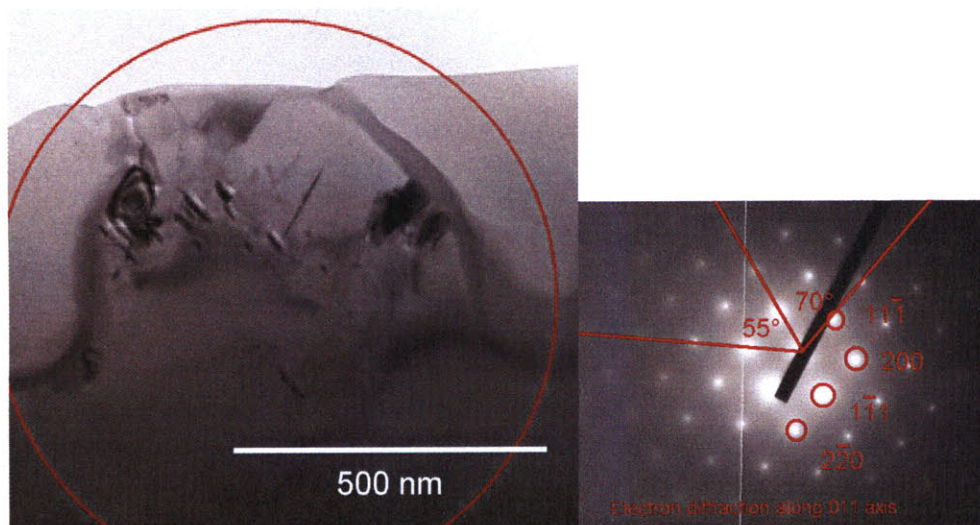


Fig. 3.8: Selected area electron diffraction over a large area in high-temperature annealed material. The electron diffraction pattern is characteristic of a largely single-crystalline region of silicon.

Figure 3.8 shows a selected area diffraction pattern from a peak region in the black silicon annealed at 950°C. The pattern is characteristic of single-crystalline silicon [5](2.3). Notice, however, that a large portion of the selected area is the unaltered substrate. Since the diffraction intensity per spot from a large single-crystalline region is greater than that of a polycrystalline region, it is possible that the surface part of this peak is in fact also polycrystalline, but that this does not show up well in the selected area diffraction. Although electron diffraction is a useful tool, it could be that the nature of black silicon is too disordered to allow definitive results from electron diffraction, except to distinguish between crystalline, amorphous and polycrystalline regions.

3.2.4 Comparison of TEM and electron diffraction results

The TEM images of samples A, B and C all showed the black silicon surface to consist of a collection of peaks with the continuous layer of altered material across the whole specimen. However, it did was not possible to definitively establish

any obvious correlation between the microstructure as observed in the TEM and the annealing temperature. While it did appear that sample C had larger single-crystalline regions than either samples A or B, the total area of material investigated was too small to reach any conclusion about exactly how the annealing temperature affects the sample.

Another difficulty with the TEM results was that it was impossible to create very thin sections that would have allowed better imaging of the grain structure. During ion-milling, the M-bond glue was invariably milled away. The regions of the sample closest to the vertex of the wedge were the thinnest, but in this region, the black silicon structure was also *laterally* milled away to a great extent, resulting in a smooth, featureless silicon surface. In future work, it would be advisable to use more resilient glue between the layers of the sample, or a focused-ion beam sample preparation method as described in section 4.2.3.

Although no definitive trend was established between annealing time and morphology, there is still plenty of useful information to be gained from the TEM images. For example, the presence of dark inclusions is an interesting fact that could be connected with the mechanism of photoabsorption. Also, the identification of a clear interface between the altered regions of the surface and the underlying substrate could help with the modeling of the process in which black silicon is made.

3.3 STEM and EDX analysis

3.3.1 Introduction

Dark-field STEM allowed imaging of the samples with heightened chemical contrast in comparison to conventional bright-field TEM. The goal of the STEM analysis was to see where the unusually high concentrations of selenium were within the black silicon. The instrument used, a JEOL 2010F, was not a dedicated scanning transmission electron microscope and was therefore difficult to calibrate, resulting in relatively low-resolution images. The mappings that are shown in Figs. 3.9, 3.10 and 3.11 were conducted of periods of time ranging from 10 minutes to 1 hour, depending on the intensity of the X-ray signal.

The samples that were looked at were the as-produced black silicon and the material annealed at 950°C, as is described in sections 3.2.2-3.2.3.

3.3.2 As-prepared material

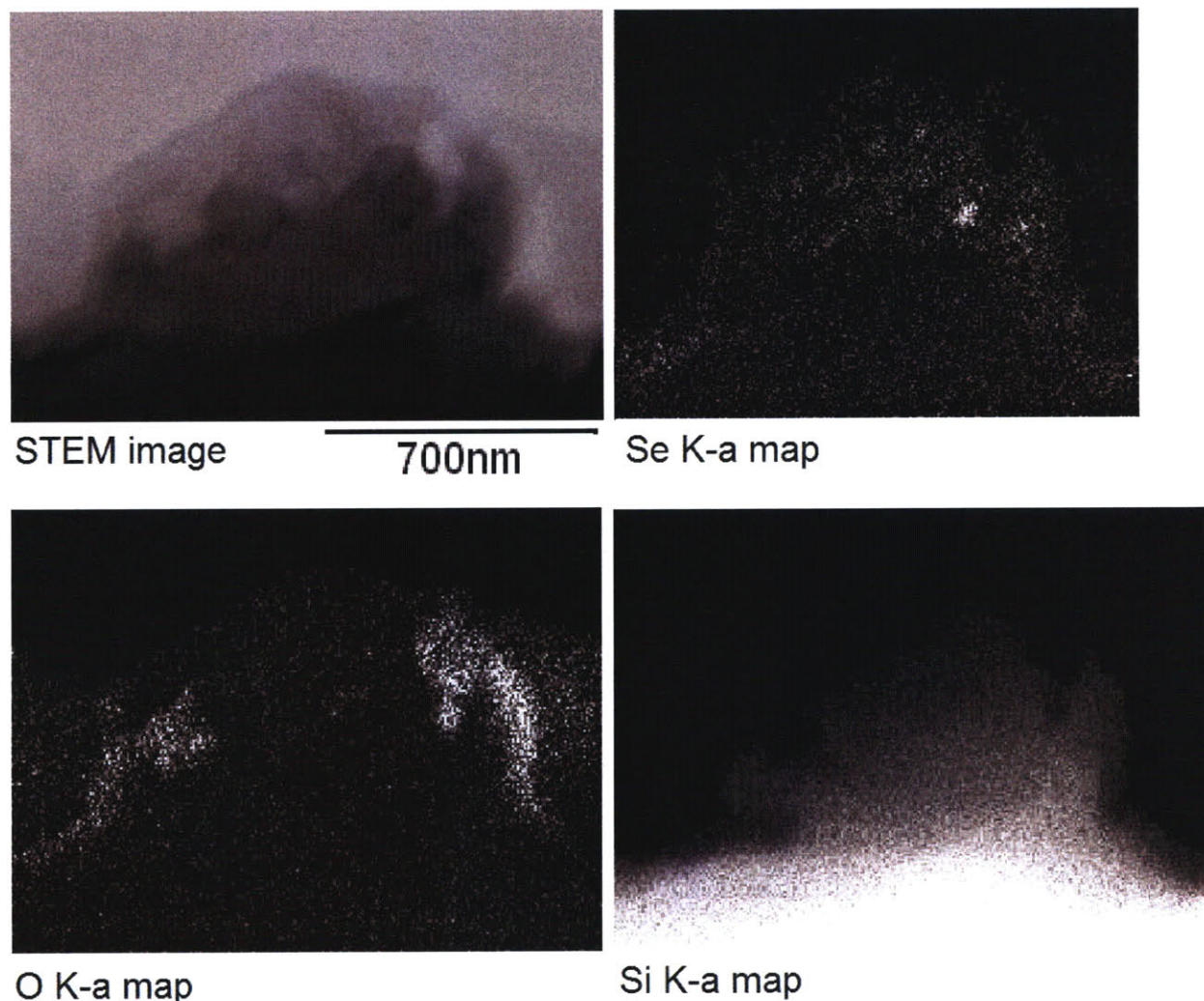


Fig. 3.9: Bright-field STEM image of a peak region in as-prepared material with accompanying EDX maps of selenium, oxygen and silicon. The amorphous layer on the surface of the sample can be identified as an oxide. Selenium concentration seems to be localized around dark areas in the bright-field STEM.

Figure 3.9 shows a typical EDX spectral mapping result from the as-prepared black silicon sample. All X-ray maps were taken using the characteristic K α X-ray energy (abbreviated as K-a in Fig. 3.9) of each element. The oxygen map shows clearly that the amorphous region surrounding the peak is oxidized silicon. Silicon naturally forms a layer of oxide when in contact with air at room temperature. One

can also see from the lack of an oxide layer at the top of the peak that the top of the peak has been milled away in the ion milling process.

The selenium map in Fig. 3.9 shows selenium mostly residing within a region 500 nm into the surface of the peak. Also, there appears to be a concentrated region of selenium to the right of the very center of the peak. This could be one of two things: either a piece of selenium that survived the laser ablation process and is stuck inside the silicon as a solid piece of selenium, or a particle of a selenium rich phase, such as SiSe or SiSe₂.

The selenium map in Fig. 3.9 shows that the selenium is mostly or entirely present in the region of the material that appears in the TEM to have been altered from its original state in the laser ablation process. The selenium signal in the single-crystalline substrate appears to be very low and indistinguishable from the random background noise.

3.3.3 Material annealed at 950°C

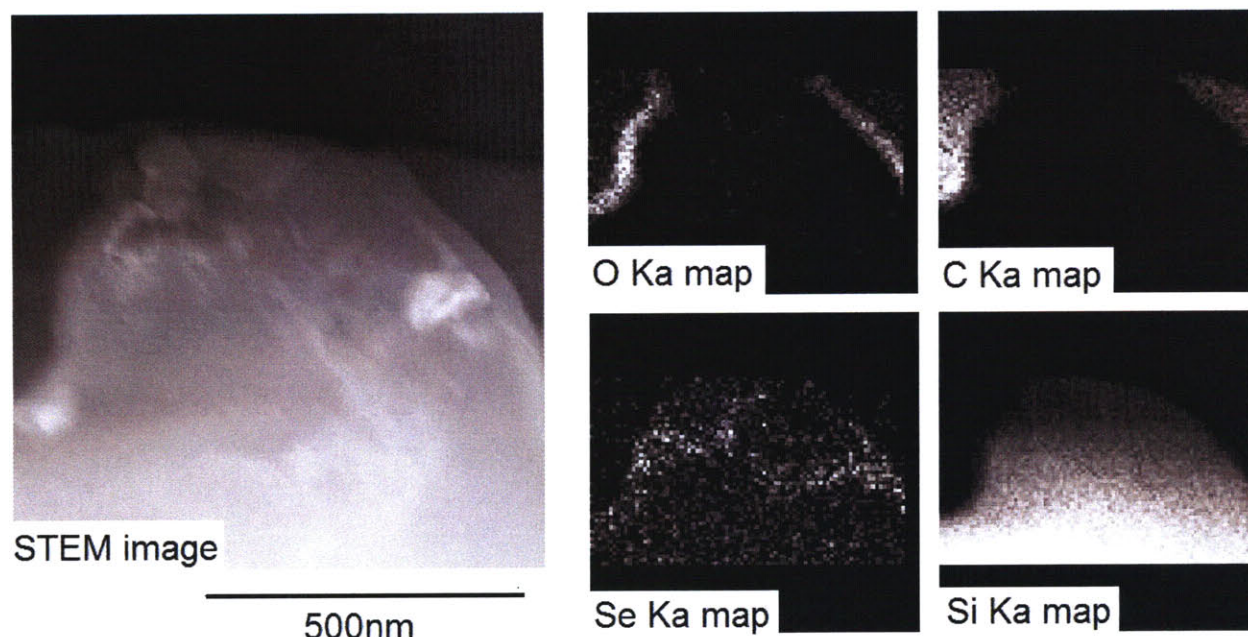
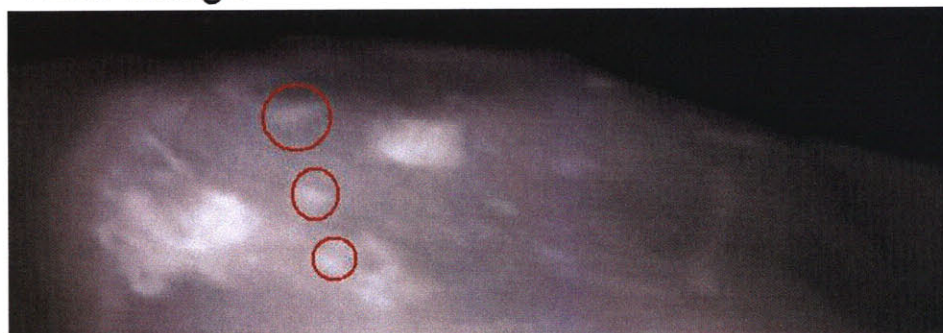


Fig. 3.10: Left: Dark-field STEM image of a peak in the 950°C annealed sample, with visible chemical contrast. Right: EDX maps of oxygen, selenium, carbon and silicon. The chemical map of selenium appears to be related to the bright areas in the DF-STEM image.

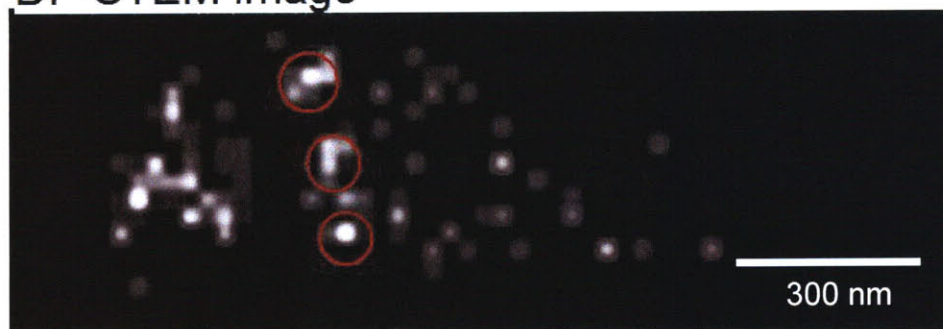
Figure 3.10 shows maps of oxygen, carbon, selenium and silicon throughout a peak in the 950°C annealed sample. The amorphous layer that covers the peak in the image is shown to be oxidized silicon. The carbon map shows that, as expected, the regions to the left and right of the peak are the carbon-based M-bond adhesive that was used. The selenium map indicates that much of the selenium resides in a band across the center of the peak: near the interface between the unaltered substrate and the altered region. This was also the region that tended to contain the faceted inclusions seen in Fig. 3.7. Note that the X-ray intensity in the silicon map decreases towards the top of the peak. This is due to the sample being thinner here and emitting fewer X-rays.



TEM image



DF-STEM image



Se EDX mapping

Fig. 3.11: TEM, STEM and EDX images of one peak. A correlation between dark inclusions seen in the TEM and higher concentrations of selenium is observed.

In Fig. 3.11 we see the same peak imaged in regular bright field TEM, in dark-field STEM mode and using Se-specific EDX mapping. There are three dark regions in the TEM picture that show up as locally high concentrations of selenium.

This suggests that the dark inclusions visible in the TEM images are in fact dark due to locally high concentrations of selenium.

There are several possibilities for what the selenium-rich regions could be. They could be chunks of pure selenium from the original coating caught inside the silicon during the laser ablation process. Alternatively they could be a selenium-rich phase that segregated out of the silicon lattice during the solidification. The documented silicon-selenium phases are SiSe_2 , which is a stable, amorphous phase similar to SiO_2 . SiSe is a phase that is stable only at high temperatures. A phase diagram of the Si-Se system can be seen in Fig. 3.12.

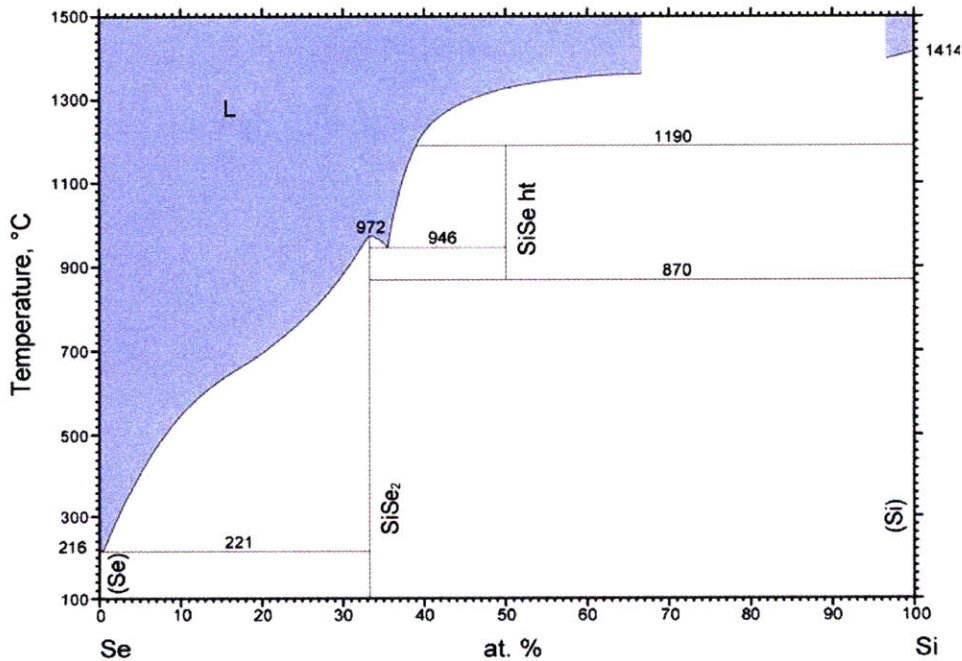


Fig. 3.12: Phase diagram of silicon-selenium system. Possible phases include SiSe_2 (stable phase) and SiSe (stable at high temperature). Black silicon likely contains a selenium-silicon compound within the silicon matrix. Diagram taken from reference [3].

Silicon diselenide has been found to absorb light in the infrared spectrum, acting as an indirect band-gap semiconductor. However, the absorption coefficient of

SiSe₂ is about 20-40cm⁻¹ in the infrared [6]. This is a relatively low, which suggests that the high absorptivity of black silicon is due to more complex factors than simple absorption by SiSe₂ precipitates.

4 Summary and future work

4.1 Brief summary of findings

Selenium based black silicon was viewed using cross-sectional transmission electron microscopy and scanning transmission electron microscopy. Procedures were developed to prepare TEM samples of black silicon using tripod polishing and ion beam milling. Also, energy dispersive X-ray spectroscopy was performed. It was found that the material has polycrystalline regions close to the surface, with single crystalline grains of diameters ranging from about 20-400 nm. The shape and dimension of the peaks appeared to vary considerably within one specimen. There also appeared to be a clear interface between the laser-altered region and the unaltered substrate. It was also found that the material contained selenium-rich particulate inclusions. It is not yet clear whether it is these particles that affect the optical properties of the material.

4.2 Future work

4.2.1 Cathodoluminescence microscopy

Cathodoluminescence electron microscopy is a technique where an electron beam is scanned across a sample and visible to infrared light is collected. This light is the result of excitations of electrons jumping across the band gap of a material. This allows characterization of the photonic properties at a high resolution. Future work could involve using cathodoluminescence, either in an SEM or an STEM to see

where the optically active regions of the material lie. This could establish a link between the remarkable optical properties of black silicon and its interesting microstructure.

4.2.2 High-angle dark-field scanning electron microscopy (HAADF-STEM)

High-angle dark-field STEM imaging is similar to conventional dark field STEM imaging, except that only electrons scattered at relatively high angles are detected. This eliminates completely the diffraction contrast. Contrast formed in this technique arises exclusively from the average atomic number present in the material in different locations. This is why the technique is also known as Z-contrast imaging, where 'Z' refers to the atomic numbers of the sample.

4.2.3 Focused ion-beam (FIB) sample preparation

Sample thickness was a large limitation in the investigation presented in this thesis. The thickness made it difficult to obtain high-resolution images of the material that clearly showed what the microstructural features were. One more recent advance that has made transmission electron microscopy more accessible to researchers is the use of focused ion beam TEM sample preparation. The principle behind this technique is to mill holes into a sample using a focused beam of gallium ions. This is done in such a way as to completely remove all material, except in a thin (~10 nm) region. In this way a thin section is prepared, as shown in Fig. 4.1.

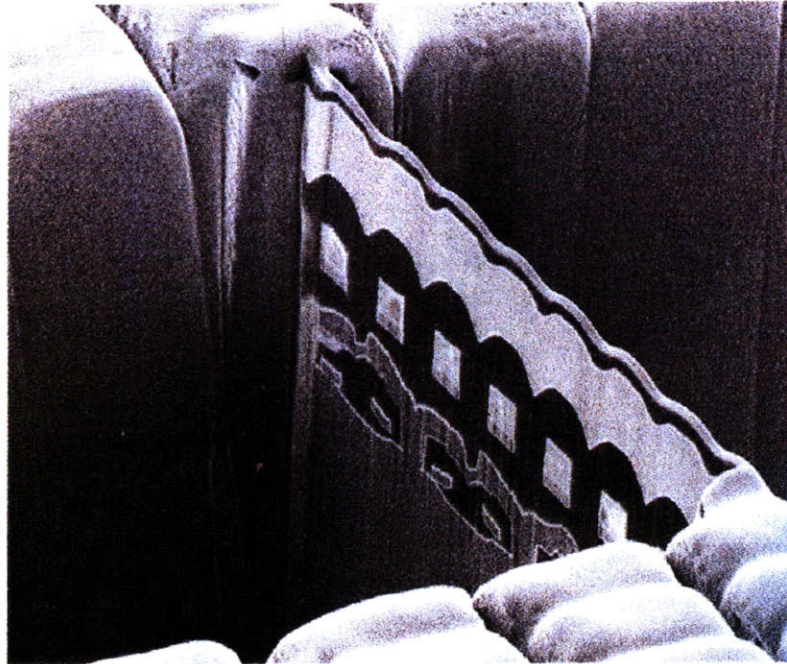


Fig. 4.1: SEM micrograph of a thin TEM cross-section milled out of a structured material using focused ion-beam (FIB) sample preparation technique. Taken from [10].

The use of a focused ion beam would allow creation of more high-quality samples. This would allow quantitative EDX studies, as well as TEM defect analysis to be done in the future.

References

- [1] Tull, B., *Femtosecond Laser Ablation of Silicon: Nanoparticles, Doping and Photovoltaics*, Ph.D. Thesis, Harvard University, (2007)
- [2] Carey, J., *Femtosecond-laser Microstructuring of Silicon for Novel Optoelectronic Devices*, Ph.D. Thesis, Harvard University (2004)
- [3] Okamoto H., *Se-Si (Selenium-Silicon)*, J. Phase Equilib, Vol. 21, pp.499 (2000)
- [4] Gradečak, S., *Structural and optical properties of laterally overgrown gallium nitride studied by transmission electron microscopy*. Ph. D. thesis, École Polytechnique Fédérale de Lausanne, (2003)
- [5] Williams, D. & Carter, B. *Transmission Electron Microscopy*, New York: Springer Science (1996)
- [6] Hauschild, E., Kannewurf, C., *Optical transmission in single-crystal silicon diselenide*, J. Phys. Chem. Solids, Vol. 30, pp. 353–357 (1969)

- [8] Ayache, J., Beaunier, L., Boumendil, J., Ehret, G., Laub, D., *Sample preparation guide for transmission electron microscopy*, Publications de l'Université de Saint-Etienne, (2009)
- [9] McCaffrey, J. P., Phaneuf, M. W., Madsen, L. D., *Surface damage formation during ion-beam thinning of samples for transmission electron microscopy*, Ultramicroscopy, Vol. 87, pp. 97–104 (2001)
- [10] Gradečák, S., *Course 3.074: Imaging in materials*, course materials, Massachusetts Institute of Technology (2009)
- [11] Muso, *Energy-dispersive X-ray spectroscopy*, Diagram.
http://en.wikipedia.org/wiki/Energy-dispersive_X-ray_spectroscopy, retrieved May 2009. Licensed under GPL.